Bursty bulk flows and dipolarization in MHD simulations of magnetotail reconnection

J. Birn,[1] R. Nakamura,[2] E. V. Panov,[2] and M. Hesse[3]

Received 2 September 2010; revised 17 November 2010; accepted 30 November 2010; published 22 January 2011.

[1] Using three-dimensional MHD simulations of magnetic reconnection in the magnetotail, we investigate the fate of earthward bursty bulk flows (BBFs). The flow bursts are identified as entropy-depleted magnetic flux tubes ("bubbles") generated by the severance of a plasmoid via magnetic reconnection. The onset of fast reconnection coincides closely with a drastic entropy reduction at the onset of lobe reconnection. The fact that, in the simulation, the Alfvén speed does not change significantly at this time suggests that the destabilization of ballooning/interchange modes is important in driving faster reconnection as well as in providing cross-tail structure. In the initial phase, the BBFs are associated with earthward propagating dipolarization fronts. When the flow is stopped nearer to Earth, the region of dipolarization expands both azimuthally and tailward. Tailward flows are found to be associated with a rebound of the earthward flow and with reversed vortices on the outside of the flow. Earthward and tailward flows are also associated with expansion and contraction of the near plasma sheet. All of these features are consistent with recent satellite observations by Cluster and the Time History of Events and their Macroscopic Interactions during Substorms (THEMIS) mission.

Citation: Birn, J., R. Nakamura, E. V. Panov, and M. Hesse (2011), Bursty bulk flows and dipolarization in MHD simulations of magnetotail reconnection, *J. Geophys. Res.*, *116*, A01210, doi:10.1029/2010JA016083.

1. Introduction

[2] Satellite observations in the magnetotail [e.g., *Baumjohann et al.*, 1990; *Angelopoulos et al.*, 1992, 1994; *Sergeev et al.*, 1996; *Schödel et al.*, 2001a, 2001b; *Petrukovich et al.*, 2001] have demonstrated that the major transport of mass, energy, and magnetic flux in the plasma sheet occurs in a bursty fashion, associated with "bursty bulk flows" (BBFs). BBFs in the plasma sheet are fast flows (several hundreds of kilometers per second) of typically 10 minutes' total duration with individual peaks of the order of 1 minute [*Angelopoulos et al.*, 1992]. They tend to occur more frequently during active times but can occur also in the absence of substorms. The flows occur both in the high-beta central plasma sheet (beta is the ratio of plasma pressure over magnetic pressure), where they have a significant component perpendicular to the magnetic field, and in the low-beta plasma sheet boundary layer, where they are strongly field-aligned [e.g., *Petrukovich et al.*, 2001]. These occurrences may be related to different activity phases, for instance, substorm expansion versus recovery. However, central plasma sheet and boundary layer flows may also represent different parts of the same earthward convecting flux tube. This can be inferred from basic conservation laws [*Schindler and Birn*, 1987].

[3] Fast earthward flows are frequently associated with thin current sheets, which form prior to, or in association with, the onset of the flow [e.g., *R. Nakamura et al.*, 2002a; *Asano et al.*, 2004a, 2004b] and with an increase of the northward magnetic field component B_z (dipolarization) in the leading part [e.g., *Baumjohann et al.*, 1990; *Angelopoulos et al.*, 1994; *R. Nakamura et al.*, 2002b; *Runov et al.*, 2009; *Nakamura et al.*, 2009]. This suggests an association with field collapse and magnetic flux pileup at the front and/or in the stopping region [*Hesse and Birn*, 1991b; *Shiokawa et al.*, 1997; *Runov et al.*, 2009; *Nakamura et al.*, 2009].

[4] Steady-state models of magnetotail transport or convection for realistic tail configurations are shown to be inconsistent with the combined conditions of frozen-in magnetic flux and mass and entropy conservation [*Erickson and Wolf*, 1980; *Schindler and Birn*, 1982]. Thus it appears that the depletion of closed magnetic flux tubes by some process(es) plays a crucial role in permitting their transport from the more distant to the nearer tail. Accordingly, *Pontius and Wolf* [1990] suggested that the earthward flow bursts were associated with magnetic flux tubes of reduced mass and entropy content and that the depletion might be an important factor in the earthward acceleration through interchange instability-generated buoyancy forces. *Chen and Wolf* [1993, 1999] supported this prediction through more quantitative approaches.

[5] The most plausible cause for depleted flux tubes and BBFs in the magnetotail is spatially and temporally local-

[1]Space Science and Applications Group, Los Alamos National Laboratory, Los Alamos, New Mexico, USA.
[2]Space Research Institute, Austrian Academy of Sciences, Graz, Austria.
[3]NASA Goddard Space Flight Center, Greenbelt, Maryland, USA.

Copyright 2011 by the American Geophysical Union.
0148-0227/11/2010JA016083

ized reconnection [e.g., *Sergeev et al.*, 1992; *Nagai et al.*, 1998; *Øieroset et al.*, 2000; *Shay et al.*, 2003; *Forsyth et al.*, 2008], which severs and ejects a part of closed flux tubes, the plasmoid [*Hones*, 1977], and also generates fast flows. Possible alternative formation processes include the loading of flux tubes with preexisting reduced entropy content or entropy losses to the ionosphere. In addition to enabling the penetration of a depleted flux tube, interchange modes associated with entropy depletion could also play a role in providing cross-tail structure to an initially unstructured earthward beam, as demonstrated in hybrid simulations [*M. S. Nakamura et al.*, 2002], or even in initiating fast flows [e.g., *Pritchett et al.*, 1997; *Pritchett and Coroniti*, 2000, 2010; *Wu et al.*, 1998; *Bhattacharjee et al.*, 1998a, 1998b; *Cheng and Lui*, 1998; *Miura*, 2001].

[6] Three-dimensional MHD simulations have confirmed that entropy reduction is indeed a crucial factor in enabling earthward transport of magnetic flux tubes [*Birn et al.*, 2004b], although the speeds of depleted flux tubes in these simulations without underlying reconnection were more modest than predicted by *Pontius and Wolf* [1990] and *Chen and Wolf* [1999]. *Birn et al.* [2004b] also confirmed the formation of a field-aligned current system of region 1 sense (earthward on the dawnward edge, tailward on the duskward edge), as postulated in previous models, and a pressure enhancement closer to the Earth. Both features are consistent with observed near-Earth signatures of flow bursts related to auroral streamers [e.g., *Fairfield et al.*, 1999; *Lyons et al.*, 1999; *Zesta et al.*, 2000; *Nakamura et al.*, 2001a, 2001b; *Sergeev et al.*, 2004; *Grocott et al.*, 2004].

[7] Here we note that entropy in this context is typically measured by the quantity PV^{γ}, where P is the plasma pressure, $V = \int ds/B$ is the volume of a flux tube of unit magnetic flux, and $\gamma = 5/3$ is the adiabatic constant [e.g., *Wolf et al.*, 2006]. This definition is suitable for equilibrium states, when P is constant along field lines. In nonequilibrium cases, the quantity PV^{γ} can be generalized to an integral

$$S = \int P^{1/\gamma} ds/B, \tag{1}$$

where the integration is taken along a field line from one boundary to the other. This quantity is strictly conserved in ideal MHD provided that there is no inflow or outflow through the boundary, but it is also found to be well conserved on Alfvénic timescales in particle simulations, except for possible changes from reconnection [*Birn et al.*, 2006].

[8] A strict observational proof that entropy depletion is associated with flow bursts is rather difficult, as the evaluation of the flux tube volume or the quantity S requires knowledge of the three-dimensional magnetic field structure. However, using plausible analytic field models, *Wolf et al.* [2006] were able to provide estimates of reduced entropy in rapidly earthward moving flux tubes in association with two substorms.

[9] Using 3-D MHD simulations, *Birn et al.* [2009b] further confirmed that the amount of depletion is an important factor in determining the depth of penetration and the speed of collapsing depleted flux tubes. In this paper, we address further the fate of depleted flux tubes when they are braked in the inner magnetosphere or the near tail. Our investigations are based on 3-D MHD simulations in which depletion is caused by localized reconnection. The simulation studies are compared with results from data analyses particularly on the basis of Time History of Events and their Macroscopic Interactions during Substorms (THEMIS) mission observations. Specifically, we investigate temporal variations of the normal magnetic field B_z (dipolarizations), the occurrence of tailward flows with positive B_z, and the spatial structure of fast flows and their evolution.

2. Overview of the Numerical Simulation

[10] In the following discussion, we use dimensionless units, based on a characteristic magnetic field strength B_c, velocity v_c, and scale length L_c. For illustration we use

$$B_c = 20\,\mathrm{nT},\ v_c = 1000\,\mathrm{km/s},\ L_c = 10,000\,\mathrm{km} \approx 1.6R_E. \tag{2}$$

These values lead to a time unit t_c = 10 s, and density n_c = 0.2 cm^{-3}. We use (mostly) standard international (SI) units with common notations. Our coordinate system is chosen such that x is positive sunward (earthward), y is duskward, and z is northward.

2.1. Initial State

[11] The numerical simulation used for this study was part of a comparison of the evolution of low-shear stretched fields, appropriate for the magnetotail, with high-shear, initially force-free, magnetic fields, appropriate for the solar corona [*Birn et al.*, 2009a] and solar flare eruptions. Our initial state was derived from the explicit three-dimensional equilibrium models given by *Birn* [1987]. A 3-D dipole magnetic field with a location of the dipole at x = 5 outside the earthward boundary of the simulation box was added. Since this superposition leads to fields that are no longer in exact force balance, we used a relaxation method [*Hesse and Birn*, 1993] to obtain force-balanced equilibria before starting the simulation of the dynamic evolution. A small net cross-tail magnetic field component B_y (guide field) was included but did not have a significant effect. A uniform background plasma pressure of 1% of the maximum magnetic pressure was also added, leading to $\beta \approx 0.01$ in the lobe regions.

2.2. Code

[12] The evolution of the magnetic field was studied on the basis of a one-fluid MHD code. This code consists of an explicit, finite difference, leapfrog scheme, based on two staggered meshes defined at alternate time steps [e.g., *Birn and Hesse*, 1996; *Birn et al.*, 2006]. A nonlinear grid is used to increase the resolution in the regions of interest, such that about one half of the grid points lie within the plasma sheet. A quasi-viscous term, similar to flux-corrected transport algorithms [e.g., *Book et al.*, 1975], damps oscillations on the grid scale, reduces the divergence between the quantities on the two meshes, and increases numerical stability. This algorithm is not used on the magnetic field to avoid introducing artificial diffusion and reconnection. Energy transport and conversion are governed by an adiabatic law with a ratio of specific heats γ = 5/3 but also including ohmic heating.

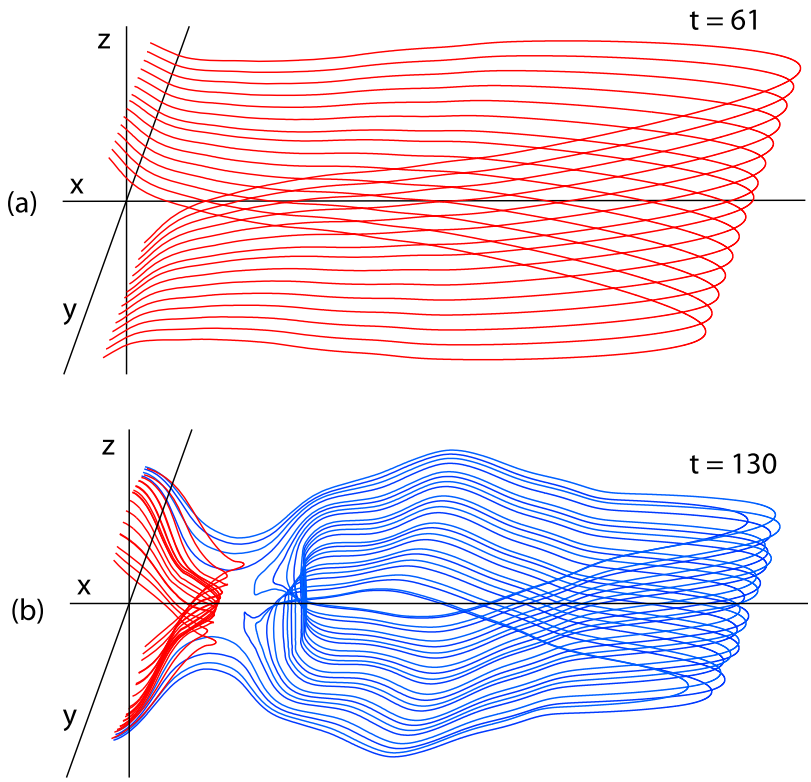

Figure 1. Perspective view of magnetic field lines (a) at $t = 61$, after the completion of the flux addition (growth phase) and at the initiation of finite resistivity, and (b) at $t = 130$, at an advanced stage of plasmoid formation and ejection.

2.3. Boundary Conditions and Initiation Phase

[13] The boundary conditions consist of solid, ideally conducting walls at each of the boundaries $x = 0$, $y = \pm y_{\max}$, and $z = \pm z_{\max}$, where all velocity components are set to zero (except for the initial phase, discussed below). Von Neumann boundary conditions ($\partial/\partial n = 0$) are imposed on density, pressure, and the tangential magnetic field components, except at the tailward boundary $x = -60$, where an open outflow condition is assumed, such that B_y and B_z are convected with the plasma flow, while the normal magnetic field B_x is held fixed. Line symmetry conditions are imposed around the x axis, such that only the half box $z \geq 0$ needs to be simulated. Our frozen-in flux boundary condition at the near-Earth boundary does not include the feedback from ionospheric current closure and the associated electric field. From an MHD stability point of view, our condition represents the most stabilizing condition. In previous simulations of a similar scenario, however, we found that the inclusion of this feedback has little effect on the tail evolution [*Hesse and Birn*, 1991a].

[14] For the present run, the number of grid cells in x, y, and z were 132, 80, and 64, respectively, for the full box. By varying the grid size and the time step, we confirmed that the basic results reported here are not affected significantly by the spatial or temporal resolution. On the basis of our chosen units in equation (2) and the dipole location, our simulation domain ranges from about $X_{GSM} = -7.8R_E$ to $X_{GSM} \approx -100R_E$ downtail.

[15] Our simulation includes a slow phase of current intensification prior to the initiation of reconnection, akin to the substorm growth phase. In this phase, magnetic flux is added to the lobe regions, decreasing in strength along the tail. Consistency also requires a slow converging motion at the near-Earth boundary $x = 0$ in the z direction toward the equatorial plane $z = 0$. This motion, with a maximum amplitude at $y = 0$, is gradually turned on and off, as described in detail by *Birn et al.* [2000]. During this phase, the resistivity is set to zero, allowing additional current to build or concentrate under the action of the slow driving. Figure 1a gives a perspective view of magnetic field lines after the completion of this phase. This flux addition leads to a modest increase in lobe field strength of ~30% but a strong concentration of current embedded within the near-Earth plasma/current sheet (Figure 3c of *Birn et al.* [2009b]), consistent with conclusions from quasi-equilibrium approaches on the basis of mass, entropy, and flux conservation [*Birn and Schindler*, 2002; *Birn et al.*, 2004a].

2.4. Onset Signals

[16] To initiate the following, eruptive phase, we imposed a localized finite resistivity, centered near the peak of the current intensification, but kept fixed in time, given by

$$\begin{aligned} \eta &= \eta_0/\cosh^2 s \\ s &= \left[\left(\frac{x-x_0}{L_x}\right)^2 + \left(\frac{y}{L_y}\right)^2 + \left(\frac{z}{L_z}\right)^2\right]^{1/2}, \end{aligned} \tag{3}$$

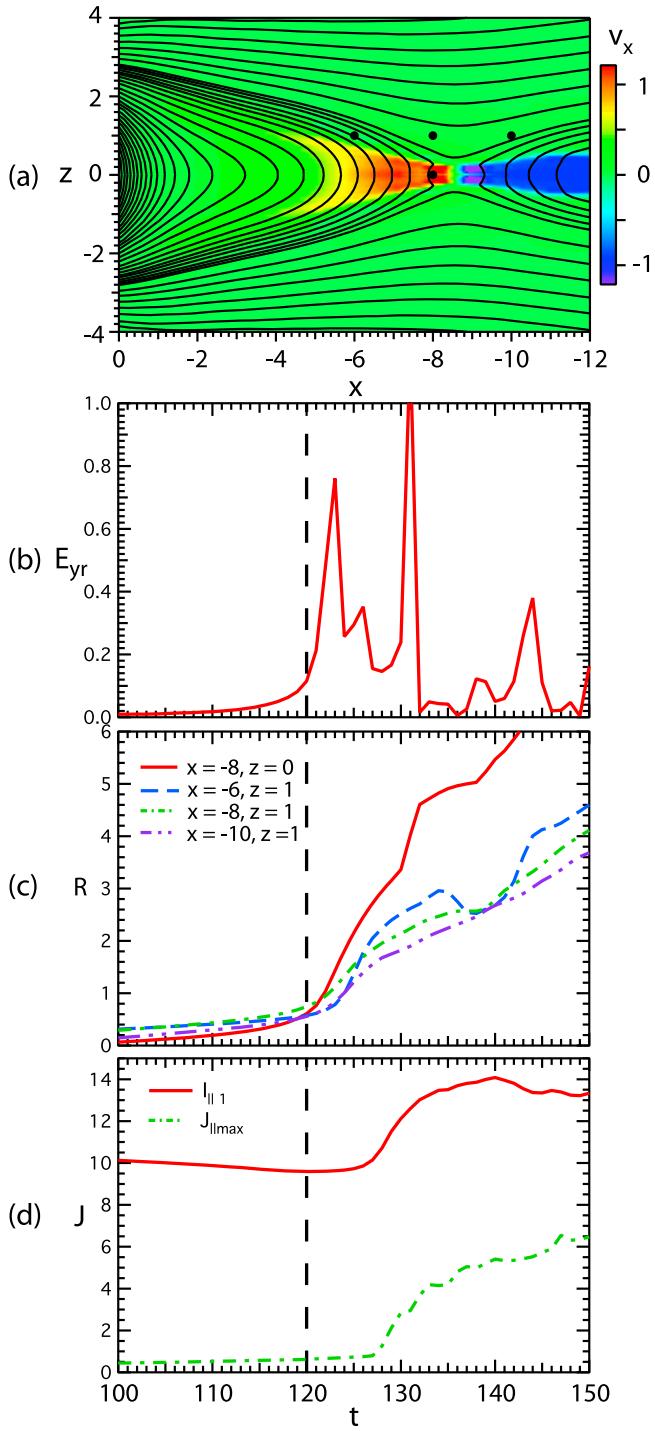

Figure 2. (a) Snapshot of the magnetic field (solid contours) and velocity v_x (color) at $t = 123$, shortly after the onset of fast reconnection, and characteristic onset features as a function of time. (b) Electric field E_y at the location of the x-line. (c) Integrated electric field $R = \int E_y dt$ at different locations indicated as dots in Figure 2a. (d) Total region 1 type (earthward) field-aligned current $I_{\|1}$, together with the maximum current density $J_{\|\max}$, at $x = 0$.

with

$$x_0 = 8, \quad L_x = 4, \quad L_y = 8, \quad L_z = 2. \tag{4}$$

The maximum value $\eta_0 = 0.005$ of the resistivity corresponds to a Lundquist number (magnetic Reynolds number) of 200 on the basis of the units of the initial state.

[17] This resistivity, in combination with the current intensification from the previous phase, leads to the onset of reconnection. The subsequent evolution of the magnetic field is illustrated by Figure 1b, indicating plasmoid formation and ejection together with a collapse of the closed field lines in the inner tail region (red lines). Since our simulation included a small net cross-tail magnetic field component, the plasmoid field lines are not closed loops but tightly wound helical field lines that initially are still connected to the earthward boundary (blue lines). Also, the reconnection site is not associated with an exact magnetic neutral line (x-line), but rather with a separator line that forms when lobe field lines begin to reconnect. However,

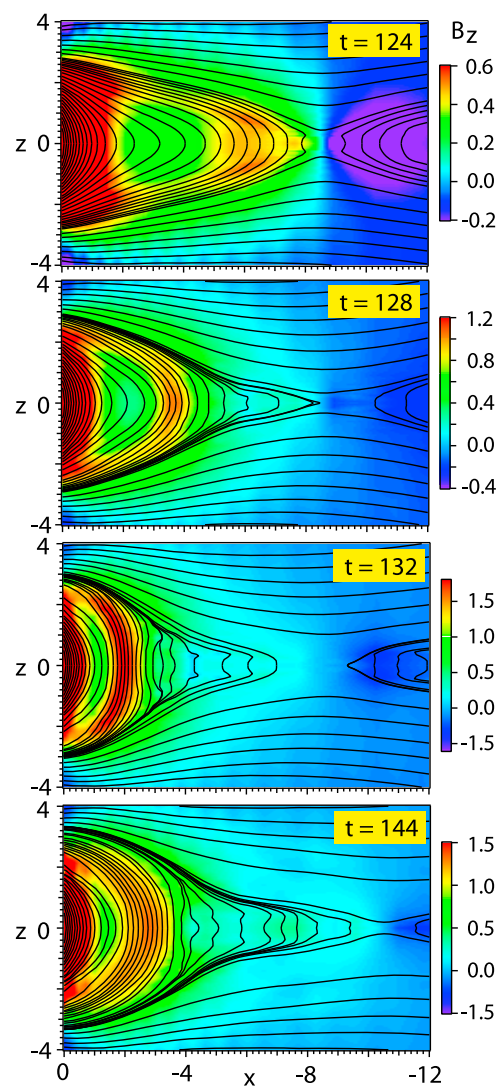

Figure 3. Magnetic field component B_z (color) and magnetic field lines in the x, z plane at different times of the MHD simulation.

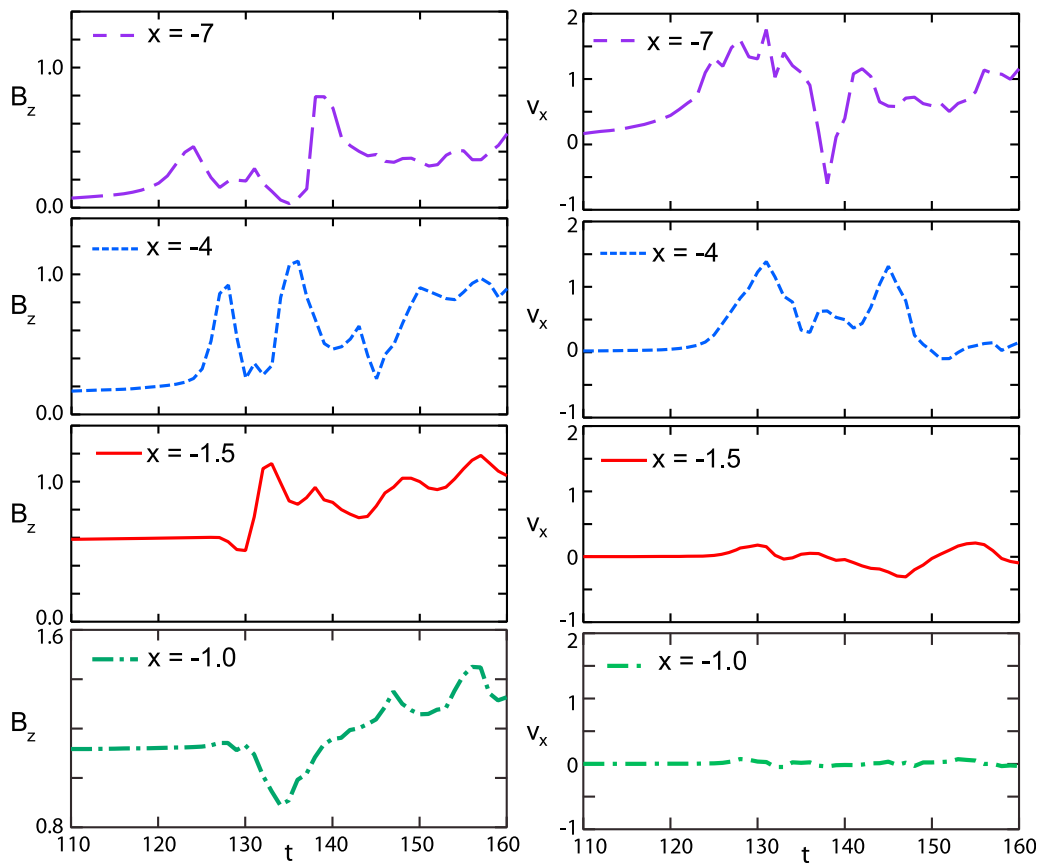

Figure 4. (left) Magnetic field component B_z and (right) velocity component v_x as a function of time at four different locations along the x axis.

since the net cross-tail field is very small and has no identifiable effect on the dynamic evolution, we disregard in our discussion the deviation from symmetry and simply use the term "neutral line" for the line where B_x and B_z vanish in the x, y plane.

[18] The time $t = 61$ marks the time when the resistivity is turned on. The neutral line forms at $t \approx 90$ near $x = -10$ (corresponding to $x_{GSM} \approx -23R_E$ for the adopted units), but rapid reconnection does not start until about $t = 120$. This is demonstrated by Figure 2, which shows characteristic signals of the onset of the dynamic evolution together with a snapshot of the magnetic field (solid contours) and velocity v_x (color) in the x, z plane (Figure 2a). Figure 2b shows the electric field at the x-line, which is a measure of the reconnection rate, indicating a rapid increase at $t \approx 120$.

[19] The likelihood that a satellite will encounter the x-line at the onset of fast reconnection is rather small. In fact, in several events observed by the THEMIS satellites, the satellite that was expected to be closest to the x-line location was not close enough to the neutral sheet to observe the onset of fast flow. In these cases, the quantity

$$R = \int E_y dt \tag{5}$$

was used as an indicator of the onset of fast magnetic flux transport, associated with reconnection [e.g., *Liu et al.*, 2009; *Angelopoulos et al.*, 2009]. We have therefore evaluated R at four different locations indicated by black dots in Figure 2a. This is shown in Figure 2c. Only one of the locations is in the region of fast flow. However, all graphs show a clear onset very close to the actual onset time of fast reconnection, although close inspection shows a slight delay for locations farther away from the x-line.

[20] Figure 2d shows the integrated earthward field-aligned current (integrated over the dawnside sector of the simulation box) and the maximum parallel current density, evaluated at the earthward boundary. These quantities are indicators of the formation of the substorm current wedge [*McPherron et al.*, 1973], associated with the auroral electrojet. These signatures are obviously delayed from the onset of fast reconnection by ~8 time units (~80 s for the adopted units). A further delay might be expected from the propagation to Earth. Such a delay is roughly consistent with conclusions from THEMIS observations [e.g., *Angelopoulos et al.*, 2008; *Liu et al.*, 2009].

3. Propagation of Dipolarization Signals

[21] Figure 3 provides an overview of the evolution of the magnetic field in the x, z plane earthward from the reconnection site, showing the magnitude of B_z (color) together with the magnetic field lines. Figure 3 demonstrates the earthward propagation of enhanced B_z after the onset of fast reconnection, the stopping nearer to Earth, and a subsequent tailward expansion.

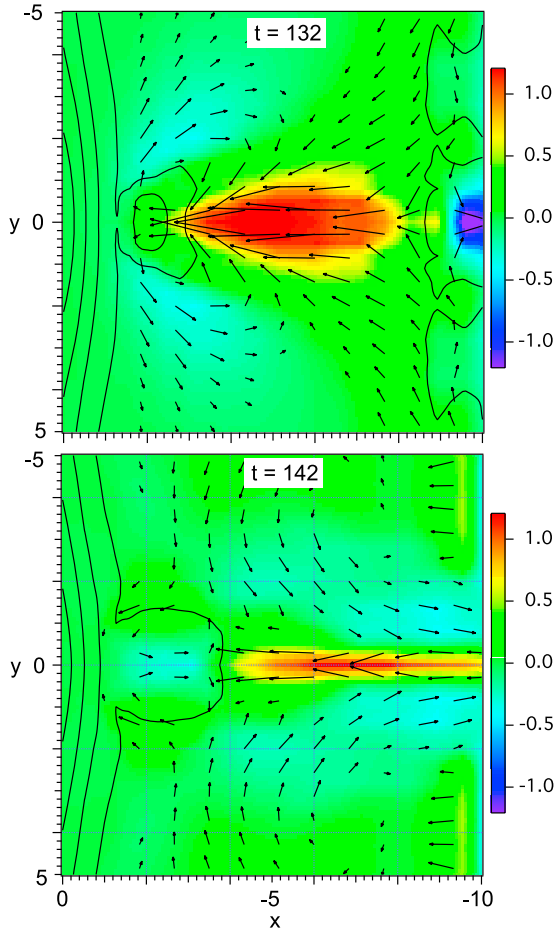

Figure 5. (top and bottom) Velocity component v_x (color) and velocity vectors in the x, y plane at two different times of the MHD simulation. Black solid lines represent contours of constant B_z, ≥ 0 with increments of 0.5. The neutral line $B_z = 0$ is farthest to the right in Figure 5 (top) and outside the box shown in Figure 5 (bottom).

[22] This sequence is demonstrated more quantitatively in Figure 4, which shows the magnetic field component B_z (left) and velocity component v_x (right) as functions of time at four different locations along the x axis. Figure 4 demonstrates the earthward propagation of a brief dipolarization signal or dipolarization front [*Runov et al.*, 2009], leading to a more permanent dipolarization first at the innermost location, where the flow is stopped, and subsequently at more and more tailward locations. This sequence is consistent with conclusions from Cluster observations [*Nakamura et al.*, 2009].

[23] It is further noteworthy that the dipolarization, i.e., the increase of B_z, may be preceded by a dip, a reduction of B_z. In the MHD simulation, this happens primarily in the stopping region closer to Earth (Figure 4, two bottom panels). This feature is commonly observed to precede dipolarizations [e.g., *Ohtani et al.*, 2004; *Runov et al.*, 2009], although the short duration of the dips indicates kinetic scales not present in the MHD simulations [*Runov et al.*, 2009]. Sometimes the observed reduction of B_z involves negative B_z. In that case, the dip may be associated with secondary reconnection involving formation of a small magnetic island or flux rope earthward of the main reconnection site [*Schindler*, 1974; *Slavin et al.*, 2003; *Sitnov et al.*, 2009]. However, this was not found in the present simulation.

4. Flow Braking and Vortex Formation

[24] Next we investigated properties of the fast flow bursts in more detail. *Ohtani et al.* [2009] found that fast tailward flows with northward B_z often followed fast earthward flows in association with dipolarization events and concluded that these flows were caused by the overshoot and rebound of earthward flows. More recently, *Panov et al.* [2010a] confirmed these conclusions by multisatellite THEMIS observations. They also inferred that both the earthward flows and the tailward flows were associated with pairs of vortices of opposite sense at their eastward and westward edges. This view is supported by our MHD simulations. Figure 5 shows two snapshots of flow vectors in the x, y plane together with the magnitude of v_x (color). Figure 5 (top) shows earthward flow associated with a clockwise vortex on the dawnside and a counterclockwise vortex on the duskside of the central flow, while Figure 5 (bottom) shows the opposite signatures associated with the reflected tailward flow.

[25] Figures 6 and 7 provide an even more direct comparison between observations and simulation. Figure 6 represents a simplified version of Figure 5 by *Panov et al.* [2010a], showing velocity and magnetic field vector components of only two THEMIS satellites, P1 and P3. Figure 7 shows velocity and magnetic field vector components obtained from the MHD simulation at locations that roughly correspond to those of THEMIS P1 and P3, respectively. The magnetic field at the outermost location, corresponding to P1, shows a brief dipolarization followed by a more permanent one a few minutes later, while the magnetic field at the innermost location (corresponding to P3) shows an immediate, more permanent dipolarization. This location is also characterized by more pronounced oscillating flows that involve even a brief upward motion falling between two earthward flow peaks. This upward motion (highlighted by green shading in Figures 7c and 7d) follows a downward motion during the first earthward flow peak (highlighted in yellow in Figures 7c and 7d). Our simulation confirms that this sequence is due to an expansion and thinning, rather than to a downward and upward motion, of the plasma sheet. This is also consistent with conclusions from THEMIS observations [*Panov et al.*, 2010b].

5. Entropy

[26] In sections 3 and 4, we have demonstrated the magnetic field and flow properties of collapsing flux tubes resulting from near-tail reconnection. In this section, we investigate the association with the entropy depletion, postulated in the bubble model [*Pontius and Wolf*, 1990], which results from the severance of a plasmoid from closed field lines (Figure 1) and the fact that the pressure on newly reconnected field lines decreases as reconnection proceeds from central plasma sheet field lines to the lobes. In the simulation discussed here, the typical lobe beta is 0.01.

[27] Figure 8 demonstrates the evolution of the entropy integral in equation (5) mapped onto the equatorial plane together with flow vectors and a color representation of the

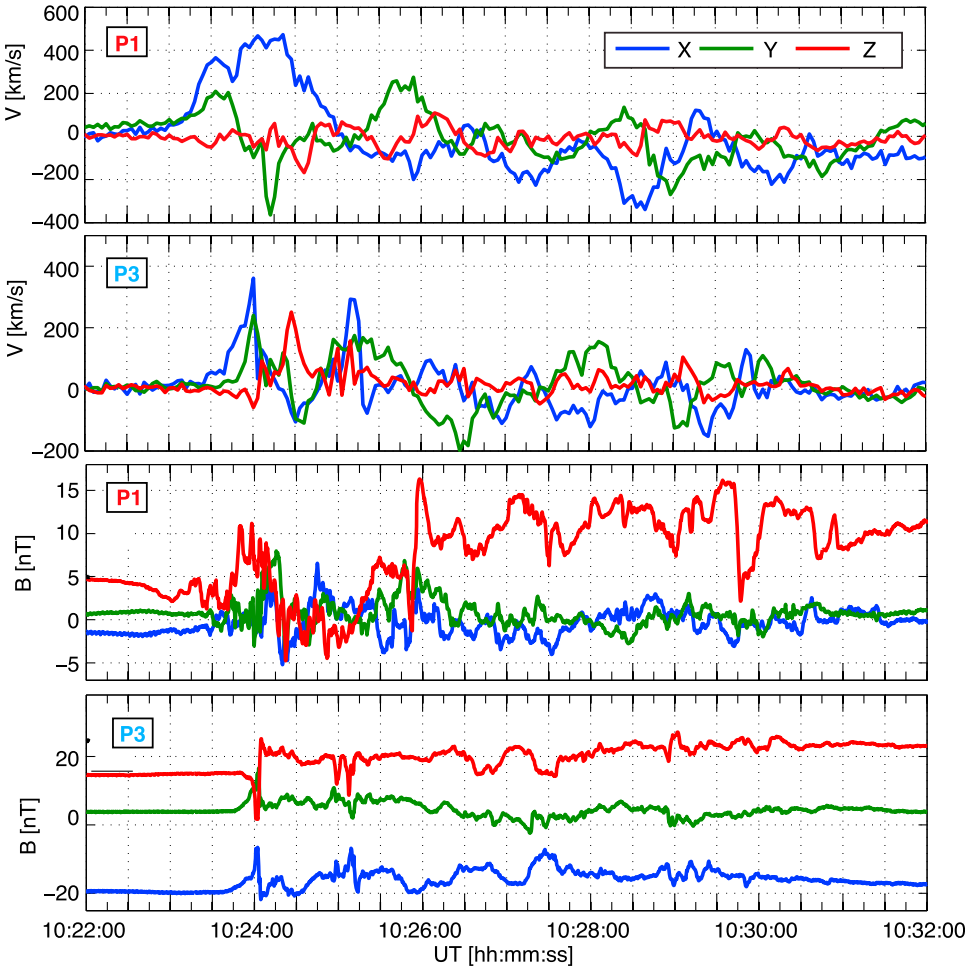

Figure 6. Velocity (top two panels) and magnetic field (bottom two panels) vector components in the *x*, *y* plane as a function of time from THEMIS satellites P1 and P3. Modified after *Panov et al.* [2010a].

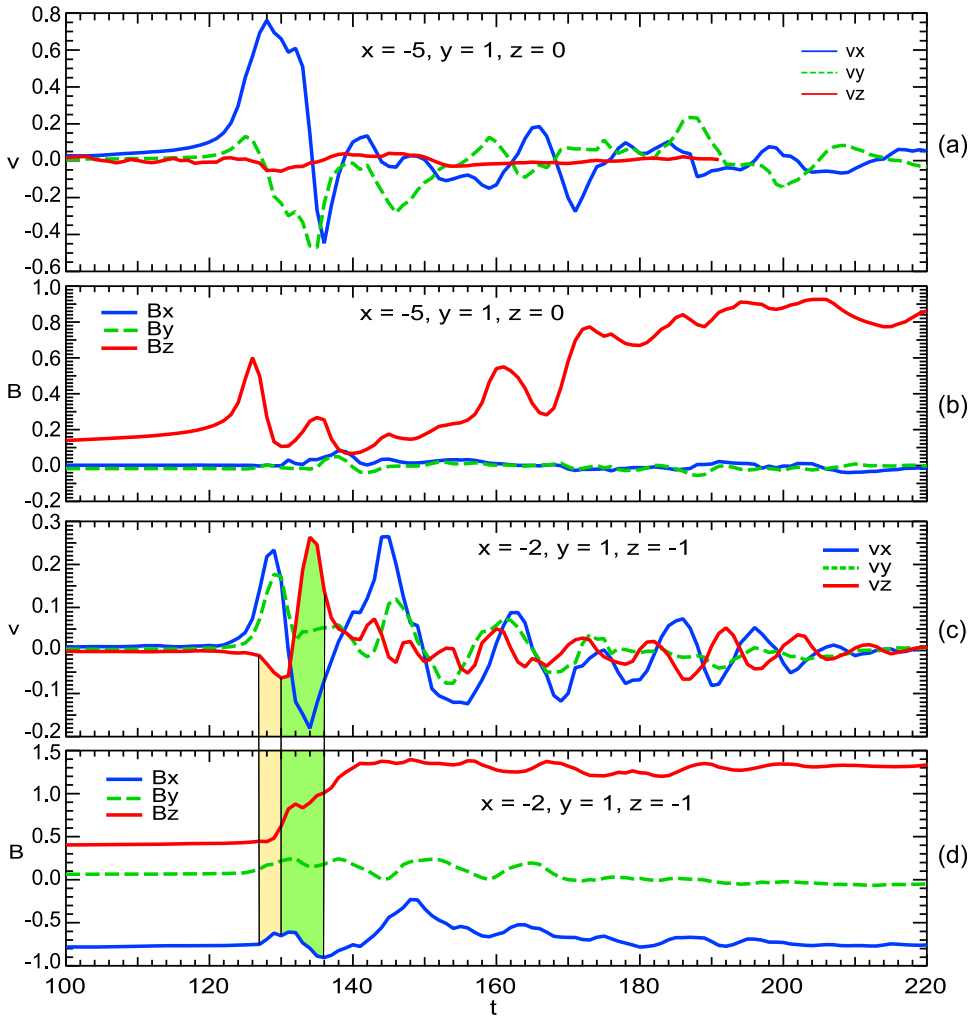

Figure 7. (a and c) Velocity and (b and d) magnetic field vector components as a function of time at two different locations obtained by the MHD simulation.

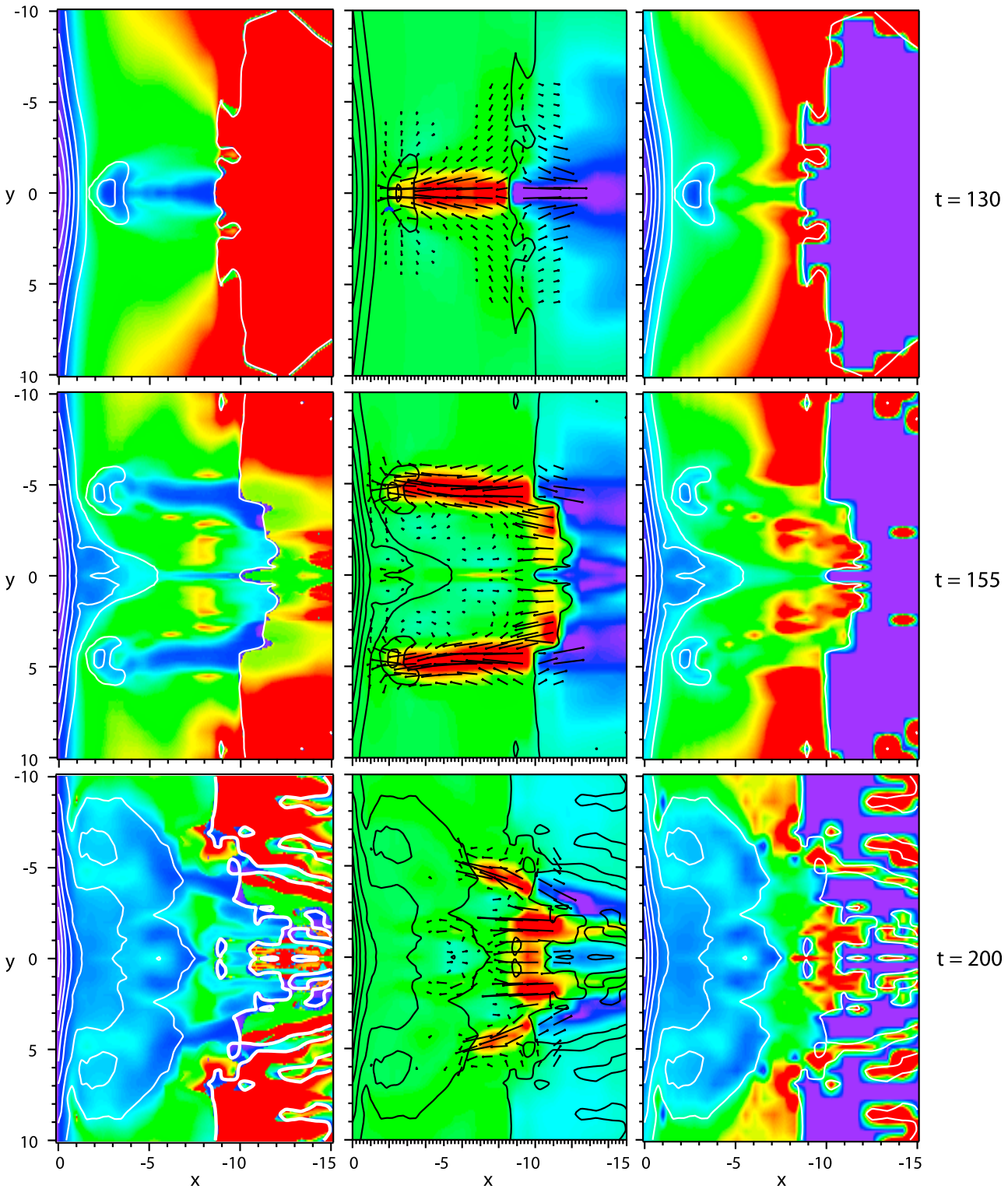

Figure 8. Entropy function $S = \int P^{1/\gamma}\, ds/B$ and flow in the x, y plane at three different times. (left) S in color as resulting from the MHD simulation, (middle) flow vectors and the magnitude of v_x (color), and (right) estimates based on the Wolf formula [*Wolf et al.*, 2006].

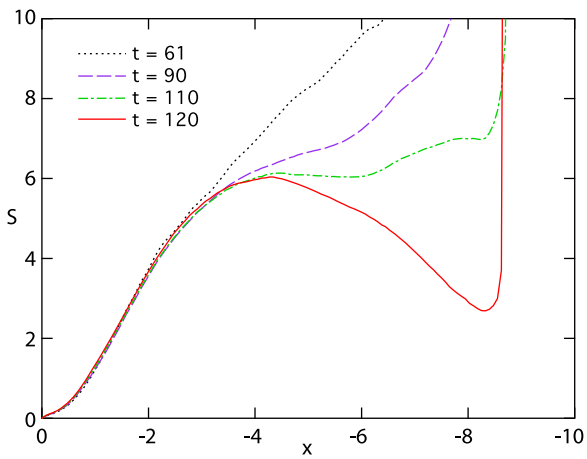

Figure 9. Entropy function $S = \int P^{1/\gamma}\, ds/B$ as a function of x along the x axis at various times, indicating the formation of a deep minimum after $t \approx 110$.

magnitude of v_x (Figure 8, middle). Figure 8 (left) shows the results from the MHD simulation and Figure 8 (right) estimates using an approximate evaluation of the entropy function on the basis of the Wolf formula [*Wolf et al.*, 2006]. The solid lines are contours of constant B_z ($\geq$0 with increments of $\Delta B_z = 0.5$, corresponding to 10 nT for the adopted units). The contour $B_z = 0$ near $x = -10$ indicates the location of the neutral line, which can become quite complicated at later times, while contours $B_z > 0$ indicate regions of enhanced B_z at the earthward fronts of the fast flows. Figure 8 covers a longer period, showing not only the initial flow burst around midnight ($y = 0$) but also two subsequent flow bursts at larger $|y|$. Note that the symmetry is imposed. Figure 8's images clearly demonstrate that the flow bursts are associated with entropy depletion (starting from the near-Earth x-line). A comparison between the columns of Figure 8 indicates that a bubble, i.e., the flux tubes of reduced entropy, may be considered comprising two parts, a "head," consisting of the region where B_z is enhanced but v_x relatively small, and a "tail," where v_x is large but B_z is small. The Wolf approximation does a very good job in capturing the heads of bubbles but not the tails. This is not surprising, because the estimate is based on the assumption of quasi-equilibrium, which is not very good in the region of fast flow. But overall the Wolf estimates do a good job in identifying bubble events.

6. Summary and Discussion

[28] Using three-dimensional MHD simulations of magnetotail reconnection, we have illustrated properties of fast earthward flows following the onset of fast reconnection. The simulation includes a preonset phase, during which a thin current sheet forms as a consequence of flux addition to the lobes. The dynamic evolution is initiated by imposing finite, spatially localized resistivity. The simulation includes a finite but very small net cross-tail component of less than 1% of the lobe field, which breaks the exact mirror symmetry but otherwise has no significant effect on the dynamic evolution. A (quasi-)neutral line ($B_z = 0$) forms in the equatorial plane ~30 Alfvén times (~5 min for some chosen characteristic units) after imposing the resistivity but fast reconnection does not start until another ~30 Alfvén times (~5 min) later.

[29] The onset of fast reconnection is indicated not only by the strong increase of the electric field at and near the reconnection site but also by the rapid increase in magnetic flux transport outside the region of fast flows. This property has been useful in inferring the onset of fast reconnection by satellites, even when they do not encounter the close vicinity of the neutral line or the region of fast earthward or tailward flows [e.g., *Angelopoulos et al.*, 2008; *Liu et al.*, 2009]. The onset of region 1 type, field-aligned currents at the near-Earth boundary of the simulation box (~15R_E earthward of the location of the neutral line) are delayed further by ~7 Alfvén times (~1.2 min).

[30] The onset of fast reconnection coincides closely with two features, the propagation of reconnection to lobe field lines and a reduction of entropy, which are closely related to the fact that reconnected lobe field lines have a drastically reduced pressure and entropy content. As demonstrated by Figure 9, the entropy reduction starts at the onset of reconnection but leads to the formation of a local minimum later, near the onset of fast reconnection. Such a minimum in the entropy distribution is the possible cause of the onset of ballooning or interchange instability [e.g., *Schindler and Birn*, 2004; *Xing and Wolf*, 2007]. Thus the onset of fast reconnection may be related to the interaction with ballooning/interchange modes which operate on a fast MHD timescale. This interpretation differs from a traditional one, in which the onset of fast lobe reconnection is attributed to the fact that the Alfvén speed in the inflow region increases when lower-density lobe fields become reconnected. To discriminate between the two interpretations, we have evaluated the Alfvén speed v_A in the inflow region. Figure 10 shows that, in the simulation, there is no significant increase of v_A at the onset of fast reconnection, which is indicated by the integrated flux function R, defined by equation (5), as in Figure 2. The negligible change in the Alfvén speed near onset is due to the fact that, in our simulation, the lobe density was not as drastically reduced as the lobe pressure. This result indicates that the entropy reduction, and the resulting change in interchange stability, may be as important as, or even more

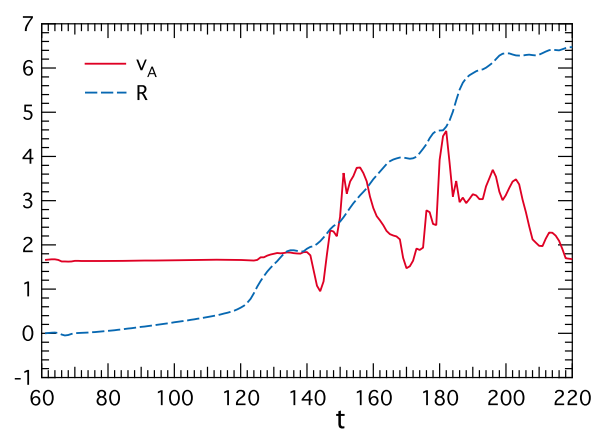

Figure 10. Alfvén speed v_A in the reconnection inflow region (solid line) and integrated reconnection electric field $R = \int E_y dt$ (dashed line) as functions of time.

important than, the change in the Alfvén speed in increasing the reconnection rate near the onset of lobe reconnection.

[31] The subsequent evolution of the fast flow is characterized by earthward propagation of a dipolarization front, as observed, for instance, by *Runov et al.* [2009], which is stopped closer to Earth, leading to an azimuthal and tailward expansion of the dipolarization signal [*Nakamura et al.*, 2009] and a tailward bounce of flow [e.g., *Ohtani et al.*, 2004; *Panov et al.*, 2010a]. Earthward and tailward flows are associated with vortex flow patterns at their eastern and western edges and expansion and contraction of the plasma sheet, consistent with conclusions from THEMIS observations [*Panov et al.*, 2010a; *Panov et al.*, 2010b].

[32] At present, it is not clear what determines the cross-tail scale size of the flow bursts, which is resolved by at least 10 grid points in the simulation and commensurate with observed scales. Linear theory predicts that the shortest wavelengths are the most unstable ballooning modes [e.g., *Schindler and Birn*, 2004]. However, the nonlinear evolution is not clear.

[33] The question also arises how sensitive our results are to various parameters, such as the resistivity model. It appears that the location of resistivity is not very critical as long as it is not outside the region of initially enhanced current density (equivalent to reduced B_z). The most sensitive part of the evolution is the breakup of an initially quasi-two-dimensional neutral line and reconnection site into localized and multiple sites, which may be affected not only by the magnitude of the resistivity but also by modifications of the initial state. This is quite similar to turbulence and may actually be viewed as the beginning of a turbulent cascade. Despite differences in details, such as number and location of flow bursts, the general features are quite repeatable: the spatial and temporal localization of the flow bursts, the association with vortices and pulsations, and the possible development of multiple reconnection and burst sites, associated with a highly corrugated x-line.

[34] **Acknowledgments.** This work was performed under the auspices of the U.S. Department of Energy, supported by NASA's MMS/SMART Theory and Modeling, Heliophysics Theory, and SR&T Programs.

[35] Robert Lysak thanks the reviewers for their assistance in evaluating this paper.

References

Angelopoulos, V., W. Baumjohann, C. F. Kennel, F. V. Coroniti, M. G. Kivelson, R. Pellat, R. J. Walker, H. Lühr, and G. Paschmann (1992), Bursty bulk flows in the inner central plasma sheet, *J. Geophys. Res.*, *97*(A4), 4027–4039, doi:10.1029/91JA02701.

Angelopoulos, V., et al. (1994), Statistical characteristics of bursty bulk flow events, *J. Geophys. Res.*, *99*(A11), 21,257–21,280, doi:10.1029/94JA01263.

Angelopoulos, V., et al. (2008), Tail reconnection triggering substorm onset, *Science*, *321*, 931–935.

Angelopoulos, V., et al. (2009), Response to comment on "Tail reconnection triggering substorm onset," *Science*, *324*, 1391.

Asano, Y., T. Mukai, M. Hoshino, Y. Saito, H. Hayakawa, and T. Nagai (2004a), Current sheet structure around the near-Earth neutral line observed by Geotail, *J. Geophys. Res.*, *109*, A02212, doi:10.1029/2003JA010114.

Asano, Y., T. Mukai, M. Hoshino, Y. Saito, H. Hayakawa, and T. Nagai (2004b), Statistical study of thin current sheet evolution around substorm onset, *J. Geophys. Res.*, *109*, A05213, doi:10.1029/2004JA010413.

Baumjohann, W., G. Paschmann, and H. Lühr (1990), Characteristics of high-speed ion flows in the plasma sheet, *J. Geophys. Res.*, *95*(A4), 3801–3809, doi:10.1029/JA095iA04p03801.

Bhattacharjee, A., Z. W. Ma, and X. Wang (1998a), Ballooning instability of a thin current sheet in the high-Lundquist-number magnetotail, *Geophys. Res. Lett.*, *25*(6), 861–864, doi:10.1029/98GL00412.

Bhattacharjee, A., Z. W. Ma, and X. Wang (1998b), Dynamics of thin current sheets and their disruption by ballooning instabilities: A mechanism for magnetospheric substorms, *Phys. Plasmas*, *5*, 2001–2009.

Birn, J. (1987), Magnetotail equilibrium theory: The general three-dimensional solution, *J. Geophys. Res.*, *92*(A10), 11,101–11,108, doi:10.1029/JA092iA10p11101.

Birn, J., and M. Hesse (1996), Details of current disruption and diversion in simulations of magnetotail dynamics, *J. Geophys. Res.*, *101*(A7), 15,345–15,358, doi:10.1029/96JA00887.

Birn, J., and K. Schindler (2002), Thin current sheets in the magnetotail and the loss of equilibrium, *J. Geophys. Res.*, *107*(A7), 1117, doi:10.1029/2001JA000291.

Birn, J., J. T. Gosling, M. Hesse, T. G. Forbes, and E. R. Priest (2000), Simulations of three-dimensional reconnection in the solar corona, *Astrophys. J.*, *541*, 1078–1095.

Birn, J., J. C. Dorelli, M. Hesse, and K. Schindler (2004a), Thin current sheets and loss of equilibrium: Three-dimensional theory and simulations, *J. Geophys. Res.*, *109*, A02215, doi:10.1029/2003JA010275.

Birn, J., J. Raeder, Y. L. Wang, R. A. Wolf, and M. Hesse (2004b), On the propagation of bubbles in the geomagnetic tail, *Ann. Geophys.*, *22*, 1773–1786.

Birn, J., M. Hesse, and K. Schindler (2006), Entropy conservation in simulations of magnetic reconnection, *Phys. Plasmas*, *13*, 092117.

Birn, J., L. Fletcher, M. Hesse, and T. Neukirch (2009a), Energy release and transfer in solar flares: Simulations of three-dimensional reconnection, *Asrophys. J.*, *695*, 1151, doi:10.1088/0004-637X/695/2/1151.

Birn, J., M. Hesse, K. Schindler, and S. Zaharia (2009b), Role of entropy in magnetotail dynamics, *J. Geophys. Res.*, *114*, A00D03, doi:10.1029/2008JA014015.

Book, D. L., J. P. Boris, and K. Hain (1975), Flux-corrected transport II: Generalizations of the method, *J. Comp. Phys.*, *18*, 248–283.

Chen, C. X., and R. A. Wolf (1993), Interpretation of high-speed flows in the plasma sheet, *J. Geophys. Res.*, *98*(A12), 21,409–21,419, doi:10.1029/93JA02080.

Chen, C. X., and R. A. Wolf (1999), Theory of thin-filament motion in Earth's magnetotail and its application to bursty bulk flows, *J. Geophys. Res.*, *104*(A7), 14,613–14,626, doi:10.1029/1999JA900005.

Cheng, C. Z., and A. T. Y. Lui (1998), Kinetic ballooning instability for substorm onset and current disruption observed by AMPTE/CCE, *Geophys. Res. Lett.*, *25*(21), 4091–4094, doi:10.1029/1998GL900093.

Erickson, G. M., and R. A. Wolf (1980), Is steady convection possible in the Earth's magnetotail?, *Geophys. Res. Lett.*, *7*(11), 897–900, doi:10.1029/GL007i011p00897.

Fairfield, D. H., et al. (1999), Earthward flow bursts in the inner magnetotail and their relation to auroral brightenings, AKR intensifications, geosynchronous particle injections and magnetic activity, *J. Geophys. Res.*, *104*(A1), 355–370, doi:10.1029/98JA02661.

Forsyth, C., et al. (2008), Observed tail current systems associated with bursty bulk flows and auroral streamers during a period of multiple substorms, *Ann. Geophys.*, *26*(1), 167–184.

Grocott, A., T. K. Yeoman, R. Nakamura, S. W. H. Cowley, H. U. Frey, H. Rème, and B. Klecker (2004), Multi-instrument observations of the ionospheric counterpart of a bursty bulk flow in the near-Earth plasma sheet, *Ann. Geophys.*, *22*, 1061–1075.

Hesse, M., and J. Birn (1991a), Magnetosphere-ionosphere coupling during plasmoid evolution: First results, *J. Geophys. Res.*, *96*(A7), 11,513–11,522, doi:10.1029/91JA00440.

Hesse, M., and J. Birn (1991b), On dipolarization and its relation to the substorm current wedge, *J. Geophys. Res.*, *96*(A11), 19,417–19,426, doi:10.1029/91JA01953.

Hesse, M., and J. Birn (1993), Three-dimensional magnetotail equilibria by numerical relaxation techniques, *J. Geophys. Res.*, *98*(A3), 3973–3982, doi:10.1029/92JA02905.

Hones, E. W., Jr. (1977), Substorm processes in the magnetotail: Comments on "On hot tenuous plasmas, fireballs, and boundary layers in the Earth's magnetotail" by L. A. Frank, K. L. Ackerson, and R. P. Lepping, *J. Geophys. Res.*, *82*(35), 5633–5640, doi:10.1029/JA082i035p05633.

Liu, J., et al. (2009), THEMIS observation of a substorm event on 04:35, 22 February 2008, *Ann. Geophys.*, *27*(5), 1831–1841.

Lyons, L. R., T. Nagai, G. T. Blanchard, J. Samson, T. Yamamoto, T. Mukai, A. Nishida, and S. Kokubun (1999), Association between geotail plasma flows and auroral poleward boundary intensifications observed by canopus photometers, *J. Geophys. Res.*, *104*(A3), 4485–4500, doi:10.1029/1998JA900140.

McPherron, R. L., C. T. Russell, and M. P. Aubry (1973), 9. Phenomenological model for substorms, *J. Geophys. Res.*, *78*(16), 3131–3149, doi:10.1029/JA078i016p03131.

Miura, A. (2001), Ballooning instability as a mechanism of the near-Earth onset of substorms, *Space Sci. Rev.*, *95*, 387–398.

Nagai, T., et al. (1998), Structure and dynamics of magnetic reconnection for substorm onsets with Geotail observations, *J. Geophys. Res.*, *103*(A3), 4419–4440, doi:10.1029/97JA02190.

Nakamura, M. S., H. Matsumoto, and M. Fujimoto (2002), Interchange instability at the leading part of reconnection jets, *Geophys. Res. Lett.*, *29*(8), 1247, doi:10.1029/2001GL013780.

Nakamura, R., W. Baumjohann, M. Brittnacher, V. A. Sergeev, M. Kubyshkina, T. Mukai, and K. Liou (2001a), Flow bursts and auroral activations: Onset timing and foot point location, *J. Geophys. Res.*, *106*(A6), 10,777–10,789, doi:10.1029/2000JA000249.

Nakamura, R., W. Baumjohann, R. Schödel, M. Brittnacher, V. A. Sergeev, M. Kubyshkina, T. Mukai, and K. Liou (2001b), Earthward flow bursts, auroral streamers, and small expansions, *J. Geophys. Res.*, *106*(A6), 10,791–10,802, doi:10.1029/2000JA000306.

Nakamura, R., et al. (2002a), Fast flow during current sheet thinning, *Geophys. Res. Lett.*, *29*(23), 2140, doi:10.1029/2002GL016200.

Nakamura, R., et al. (2002b), Motion of the dipolarization front during a flow burst event observed by Cluster, *Geophys. Res. Lett.*, *29*(20), 1942, doi:10.1029/2002GL015763.

Nakamura, R., et al. (2009), Evolution of dipolarization in the near-Earth current sheet induced by Earthward rapid flux transport, *Ann. Geophys.*, *27*(4), 1743–1754.

Ohtani, S. I., M. A. Shay, and T. Mukai (2004), Temporal structure of the fast convective flow in the plasma sheet: Comparison between observations and two-fluid simulations, *J. Geophys. Res.*, *109*, A03210, doi:10.1029/2003JA010002.

Ohtani, S., Y. Miyashita, H. Singer, and T. Mukai (2009), Tailward flows with positive B_Z in the near-Earth plasma sheet, *J. Geophys. Res.*, *114*, A06218, doi:10.1029/2009JA014159.

Øieroset, M., T. D. Phan, R. P. Lin, and B. U. Ö. Sonnerup (2000), Walén and variance analyses of high-speed flows observed by Wind in the midtail plasma sheet: Evidence for reconnection, *J. Geophys. Res.*, *105*(A11), 25,247–25,263, doi:10.1029/2000JA900075.

Panov, E. V., et al. (2010a), Multiple overshoot and rebound of a bursty bulk flow, *Geophys. Res. Lett.*, *37*, L08103, doi:10.1029/2009GL041971.

Panov, E. V., et al. (2010b), Plasma sheet thickness during a bursty bulk flow reversal, *J. Geophys. Res.*, *115*, A05213, doi:10.1029/2009JA014743.

Petrukovich, A. A., W. Baumjohann, R. Nakamura, R. Schödel, and T. Mukai (2001), Are earthward bursty bulk flows convective or field-aligned?, *J. Geophys. Res.*, *106*(A10), 21,211–21,215, doi:10.1029/2001JA900019.

Pontius, D., and R. A. Wolf (1990), Transient flux tubes in the terrestrial magnetosphere, *Geophys. Res. Lett.*, *17*(1), 49–52, doi:10.1029/GL017i001p00049.

Pritchett, P. L., and F. V. Coroniti (2000), Localized convection flows and field-aligned current generation in a kinetic model of the near-Earth plasma sheet, *Geophys. Res. Lett.*, *27*(19), 3161–3164, doi:10.1029/2000GL000107.

Pritchett, P. L., and F. V. Coroniti (2010), A kinetic ballooning/interchange instability in the magnetotail, *J. Geophys. Res.*, *115*, A06301, doi:10.1029/2009JA014752.

Pritchett, P. L., F. V. Coroniti, and R. Pellat (1997), Convection-driven reconnection and the stability of the near-Earth plasma sheet, *Geophys. Res. Lett.*, *24*(8), 873–876, doi:10.1029/97GL00672.

Runov, A., V. Angelopoulos, M. I. Sitnov, V. A. Sergeev, J. Bonnell, J. P. McFadden, D. Larson, K. Glassmeier, and U. Auste (2009), THEMIS observations of an earthward propagating dipolarization front, *Geophys. Res. Lett.*, *36*, L14106, doi:10.1029/2009GL038980.

Schindler, K. (1974), A theory of the substorm mechanism, *J. Geophys. Res.*, *79*(19), 2803–2810, doi:10.1029/JA079i019p02803.

Schindler, K., and J. Birn (1982), Self-consistent theory of time-dependent convection in the Earth's magnetotail, *J. Geophys. Res.*, *87*(A4), 2263–2275, doi:10.1029/JA087iA04p02263.

Schindler, K., and J. Birn (1987), On the generation of field-aligned plasma flow at the boundary of the plasma sheet, *J. Geophys. Res.*, *92*(A1), 95–107, doi:10.1029/JA092iA01p00095.

Schindler, K., and J. Birn (2004), MHD stability of magnetotail equilibria including a background pressure, *J. Geophys. Res.*, *109*, A10208, doi:10.1029/2004JA010537.

Schödel, R., R. Nakamura, W. Baumjohann, and T. Mukai (2001a), Rapid flux transport and plasma sheet reconfiguration, *J. Geophys. Res.*, *106*(A5), 8381–8390, doi:10.1029/2000JA900159.

Schödel, R., W. Baumjohann, R. Nakamura, V. Sergeev, and T. Mukai (2001b), Rapid flux transport in the central plasma sheet, *J. Geophys. Res.*, *106*(A1), 301–313, doi:10.1029/2000JA900139.

Sergeev, V. A., R. C. Elphic, F. S. Mozer, A. Saint-Marc, and J. A. Sauvaud (1992), A two-satellite study of nightside flux transfer events in the plasma sheet, *Planet. Space Sci.*, *40*, 1551–1572.

Sergeev, V. A., V. Angelopoulos, J. T. Gosling, C. A. Cattell, and C. T. Russell (1996), Detection of localized, plasma-depleted flux tubes or bubbles in the midtail plasma sheet, *J. Geophys. Res.*, *101*(A5), 10,817–10,826, doi:10.1029/96JA00460.

Sergeev, V. A., K. Liou, P. T. Newell, S.-I. Ohtani, M. R. Hairston, and F. Rich (2004), Auroral streamers: Characteristics of associated precipitation, convection and field-aligned currents, *Ann. Geophys.*, *22*, 537–548.

Shay, M. A., J. F. Drake, M. Swisdak, W. Dorland, and B. N. Rogers (2003), Inherently three dimensional magnetic reconnection: A mechanism for bursty bulk flows?, *Geophys. Res. Lett.*, *30*(6), 1345, doi:10.1029/2002GL016267.

Shiokawa, K., W. Baumjohann, and G. Haerendel (1997), Braking of high-speed flows in the near-Earth tail, *Geophys. Res. Lett.*, *24*(10), 1179–1182, doi:10.1029/97GL01062.

Sitnov, M. I., M. Swisdak, and A. V. Divin (2009), Dipolarization fronts as a signature of transient reconnection in the magnetotail, *J. Geophys. Res.*, *114*, A04202, doi:10.1029/2008JA013980.

Slavin, J. A., R. P. Lepping, J. Gjerloev, D. H. Fairfield, M. Hesse, C. J. Owen, M. B. Moldwin, T. Nagai, A. Ieda, and T. Mukai (2003), Geotail observations of magnetic flux ropes in the plasma sheet, *J. Geophys. Res.*, *108*(A1), 1015, doi:10.1029/2002JA009557.

Wolf, R. A., V. Kumar, F. R. Toffoletto, G. M. Erickson, A. M. Savoie, C. X. Chen, and C. L. Lemon (2006), Estimating local plasma sheet $pv^{5/3}$ from single-spacecraft measurements, *J. Geophys. Res.*, *111*, A12218, doi:10.1029/2006JA012010.

Wu, C., P. L. Pritchett, and F. V. Coroniti (1998), Hydromagnetic equilibrium and instabilities in the convectively driven near-Earth plasma sheet, *J. Geophys. Res.*, *103*(A6), 11,797–11,810, doi:10.1029/98JA00589.

Xing, X., and R. A. Wolf (2007), Criterion for interchange instability in a plasma connected to a conducting ionosphere, *J. Geophys. Res.*, *112*, A12209, doi:10.1029/2007JA012535.

Zesta, E., L. R. Lyons, and E. Donovan (2000), The auroral signature of earthward flow bursts observed in the magnetotail, *Geophys. Res. Lett.*, *27*(20), 3241–3244, doi:10.1029/2000GL000027.

J. Birn, Space Science and Applications Group, Los Alamos National Laboratory, Los Alamos, NM 87545, USA. (jbirn@lanl.gov)

M. Hesse, NASA Goddard Space Flight Center, Greenbelt, MD 20771, USA.

R. Nakamura and E. V. Panov, Space Research Institute, Austrian Academy of Sciences, A-8042 Graz, Austria.